Viscoelasticity of entangled actin networks studied by long-pulse magnetic bead microrheometry

Jorg Uhde,[1] Nikita Ter-Oganessian,[1] David A. Pink,[2] Erich Sackmann,[1] and Alexei Boulbitch[1]
[1]*Department for Biophysics, Technical University of Munich, James-Franck-Strasse 1, D-85747 Garching at Munich, Germany*
[2]*Physics Department, St. Francis Xavier University, Antigonish, Nova Scotia, Canada B2G 2W5*
(Received 12 August 2005; published 23 December 2005)

We studied the viscoelastic response of entangled actin networks using embedded microbeads driven by force pulses with amplitudes in the range from 3 to 120 pN and durations up to 60 s. We distinguished three regimes in the time dependence of the compliance $J(t)$ of the network. These were characterized by specific power laws $J(t) \sim t^{\alpha_i}$ $(i=1, 2, 3)$. In the short-time regime $(i=1)$, we observed the exponent $\alpha_1 \approx 0.75$. In the long-time regime $(i=3)$, we find that $\alpha_3 \approx 1$. For the intermediate-time interval $(i=2)$, we observed a novel dynamic regime: for all actin concentrations and all applied forces, it was characterized by the exponent $\alpha_3 \approx 0.5$. In both regimes $i=2$ and $i=3$, the compliance depended upon the actin concentration c, such as $J \sim c^{-\gamma_i}$ with $\gamma_2 \approx 1.1$ and $\gamma_3 \approx 1.4$. Using these results, we calculated the shear modulus in the frequency domain and found that the intermediate-time regime in the t domain corresponds to its plateau behavior.

DOI: 10.1103/PhysRevE.72.061916 PACS number(s): 87.16.Ka, 83.60.Df, 87.15.La

I. INTRODUCTION

Semiflexible macromolecular networks exhibit unique viscoelastic properties which determine the mechanical behavior of cells and tissues and control the dynamics of cellular processes such as adhesion and cell transport through blood vessels or bones [1]. Systematic studies of the structural and mechanical properties of these types of materials are, thus, essential in order to relate the biological functions of cells and tissues to their microstructural material properties. A promising strategy to cope with these intrinsic heterogeneously structured biomacromolecular networks and gels is to establish simplified but nevertheless realistic *in vitro* models of biomaterials and to perform comparative studies of model systems and natural materials using micromechanical tools such as micropipettes [2], atomic force microscopes [3–5], optical tweezers [6], and magnetic bead microrheometers [7–11].

Actin is a filamentous semiflexible protein and a major component of the intracellular scaffold skeleton of eukaryotic cells. Actin networks play a key role in the mechanical stability of cells and in numerous chemomechanical processes [1], such as cell locomotion on surfaces [12] and the growth of cellular protrusions [13]. The biological function of the cytoskeleton is determined by its viscoelastic properties, which are controlled by the highly heterogeneous and constantly changing structure of the network. Mechanical studies of the local viscoelastic behavior of intracellular scaffolds are absolutely essential to relate the biological function to structural and physical properties of the macromolecular networks. In the classical rheometry of technical materials, samples are subjected to homogeneous shear fields, in which local effects (such as local nonaffine deformation of the network, local nanofluidics, or microinhomogeneities) are screened, and the mechanical responses of bulk samples are studied.

Local microviscoelastic properties of actin networks have been extensively studied by a number of methods. Among these methods, one can distinguish between the so-called passive and active approaches. In passive microrheology, the viscoelastic parameters are determined by analysis of thermal fluctuations of embedded beads in terms of Einstein's theory of Brownian motion [14–21].

Under realistic biological conditions, however, forces acting on cells are usually highly inhomogeneous and are often distributed over regions with the extent comparable to those of the inhomogeneities of the cytoskeleton. To gain an insight into the viscoelastic responses of biomaterials under natural conditions, microrheological tools capable of probing the characteristic length scales have to be applied. Active microrheometry is ideally suited to examine such microviscoelastic processes.

During active microrheological experiments, a force is applied either to the cantilever tip of an atomic force microscope [3–5] or to a bead by either a laser beam (optical tweezers) [6,22] or a magnetic field (magnetic tweezers) [7–11,23,34], and the response of the object is measured in terms of the displacement of the bead or of the atomic force microscope (AFM) tip.

Pulsed-force magnetic tweezers allow one to apply unidirectional force pulses of rectangular shape to paramagnetic beads. This technique enables us to apply long (up to 60 s) pulses and to measure displacements of the beads from about 0.06 μm (corresponding to about 20% of the network mesh size) up to 600 μm. The bead displacement, $x(t)$, induced by a rectangular force pulse with amplitude f is related to the creep compliance, $J(t)$, as

$$J(t) = \frac{6\pi R x(t)}{f}, \tag{1}$$

where R is the bead radius and t is the time. Recently, we reported [35] for the first time a new type of behavior in the microrheometry of the actin network. We showed that during the forced motion of beads embedded in tightly entangled actin solutions, the compliance obeys a power law $J(t) \sim t^{0.5}$. In this paper, we report on these measurements in detail and report further results obtained by long force-pulsed microrheometry of entangled actin networks.

Earlier, we showed [35] that the response curve exhibits three regimes each of which obeys the law

$$J(t) = A_i t^{\alpha_i} + b_i. \quad (2)$$

Here $i=1, 2, 3$ denotes the short-time, the intermediate-time, and the long-time regimes, respectively; A_i are the prefactors; and b_i are the offsets with $b_1=b_2=0$ and $b_3 \neq 0$. In the short-time regime ($i=1$), we found the well-known [14,28,36,37] power law with the exponent $\alpha_1 \approx 0.75$. In the intermediate-time regime ($i=2$), the networks exhibited the power law (2) with $\alpha_2 \approx 0.5$ over two decades. In the long-time regime ($i=3$), we observed the viscouslike motion characterized by $\alpha_3 \approx 1$. We established a power law $J \sim c^{\gamma_i}$ for the variation of the creep compliance with respect to the actin concentration and found, in the intermediate-time and long-time regimes, $\gamma_2 \approx 1.1$ and $\gamma_3 \approx 1.4$, respectively. We further showed that compliance does not depend on the force pulse amplitude f in the short-time and long-time regimes as is found for small forces in the intermediate regime. However, at higher forces in the intermediate regime, the force dependence of the compliance followed the power law $J \sim f^{-\beta_2}$ with $\beta_2 \approx 0.27$. Using our compliance data, we calculated the frequency-dependent viscoelastic modulus $G(\omega)$, which also exhibited three regimes. Here, we show that the plateau regime of the storage modulus $G'(\omega)$ corresponds to the compliance $J(t) \sim t^{1/2}$, i.e., to intermediate-time regime in the t domain.

The paper is organized as follows. In Sec. II, we describe the materials and the methods. In Sec. III, we present our observations and extract the power laws which describe the enforced bead motion and calculate the viscoelastic modulus in the frequency domain from our compliance data. In Sec. IV, we summarize the results and discuss the behavior of the viscoelastic modulus and its relation to the compliance in the t domain.

II. MATERIALS AND METHODS

A. Magnetic Tweezers

All measurements were performed with a magnetic bead microrheometer (magnetic tweezers) described previously [7,32,38]. The central measuring unit consists of a sample holder and a magnetic coil [1200 turns of 0.7-mm-diameter copper wire on a core with dimensions 1 cm(diameter) $\times$5 cm(length)]. The end of the core, which is prolonged and narrows down to a sharp 60° edge, penetrates the closed sample holder with inner dimensions of 5 mm $\times$1 cm(length) $\times$0.2 mm(height) from the small side and corresponds to 100 μl of the sample volume. The complete unit is mounted on an AXIOVERT 10 microscope (Zeiss, Oberkochen, Germany). The coil current is supplied by a specialized current source built in our laboratory that is capable of generating rectangular current pulses in spite of the high induction of the coil (typically 95% of the constant current level is reached in less then 10 ms). This experimental setup makes it possible to apply rectangular force pulses, with amplitude ranging from one to a few hundred piconewtons to superparamagnetic transducer particles embedded in the actin network.

Bright field microscope images of embedded transducer beads of radius $R \approx 2.25$ μm were recorded at 70 Hz by a charge-coupled device (CCD) camera (C4880, Hamamatsu Photonics, Hamamatsu City, Japan) and digitized movies were stored directly onto the hard disk of a fast personal computer (PC) system with a RAID controller, by the use of the software OPENBOX27. The value of the actual coil current was stored together with every movie frame for later analysis. The variation of the applied force on the bead with the distance between the center of the bead and the end of the tip of the iron core was determined from independent calibration measurements of similar superparamagnetic particles in solutions of known viscosity. Using this data, we calculated the force applied to the bead at each moment of time together with the actual position of the bead. The positions of the particles were determined with an accuracy of about 10 nm by digital image processing.

Two types of systematic errors have to be considered. The first is due to an uncertainty in the initial position of the bead center point. It is only known that the starting time of the rectangular force pulse lies between the last measured time before the coil current is switched on (which we define as $t=0$) and the first data point captured after the onset of the force ($t \approx 14$ ms). This uncertainty shifts only the first measured data points to lower values of x and can be corrected as described in Ref. [39]. The second type of error may take place during the very last stage of motion when the bead approaches the magnet tip, since in this region, the force increases rapidly with bead displacement. To avoid this, we analyzed only responses for which the forces increased by less than 10%. Under this condition, the slopes of the creep compliance curves deviate by less than 10% [39].

B. Protein preparation

Monomeric G actin was prepared from rabbit skeletal muscle [40] and residual cross-linking and capping proteins were removed as described previously [41]. Actin concentrations were determined by photometry (with the extinction coefficient of $\varepsilon_{290}=0.63$ mg^{-1} cm^{-1} at $\lambda=290$ nm [42]). All measurements were performed with freshly prepared actin, which was sterile filtered and kept in G buffer [2 mM Tris-(hydroxymethyl)-aminoethane/HCl buffer (Tris-HCl), 0.2 mM $CaCl_2$, 0.2 mM DTT, 0.2 mM adenosine triphosphate (ATP), 0.005 vol.- % NaN_3 at pH 8.0] on ice for, at most, 10 days. Polymerization of G actin occurred at room temperature in F buffer (2 mM Tris-HCl, 100 mM KCl, 0.2 mM $CaCl_2$, 2 mM $MgCl_2$, 0.2 mM ascorbic acid, 0.5 mM ATP at pH 7.7) slightly modified by addition of 200 mM KCl and 10 mM of ATP and Mg^{2+}. Following the previous procedure [7], the magnetic beads (Dynabeads M-450, Dynal, Hamburg, Germany; with radius $R=2.25$ μm) were added to this solution.

C. Preparation of networks with various mesh sizes

To analyze the variation of the viscoelastic properties of the actin networks with the mesh sizes, we used five samples with actin concentrations of $c=3, 11, 19, 27, 35$ μM, which were prepared on the same day with equal polymerization

TABLE I. Concentrations and corresponding mesh sizes of actin networks.

Concentration (μM)	Concentration (g/l)	Mesh size (μm)
3	0.126	0.96
11	0.462	0.50
19	0.798	0.38
27	1.134	0.32
35	1.470	0.28

times. The average mesh sizes corresponding to the above values of concentrations are summarized in Table I. The lowest concentration is chosen in such a way that the solution forms an entangled network, while its upper limit value is determined by the solubility of the monomer.

We determined 130 response curves of 5 samples (of the different actin concentrations mentioned above). The responses of 20 to 30 beads were taken for each sample at various forces between 3 and 120 pN. The measurements started at least 40 mn after the initiation of polymerization. The maximum pulse length, τ_{max}, was restricted by the time necessary for the bead to cross the chamber. τ_{max}, therefore, depends on the force amplitude and decreased to about 10 s at $f \geqslant 100$ pN. The maximum pulse lengths for smaller forces were about 60 s.

III. RESULTS

A. Displacement of beads during the force pulse

A typical deflection of the bead *versus* time is shown in Fig. 1(a). It was obtained with a force amplitude $f=40$ pN and the force pulse duration $\tau_{max} \approx 35$ s. Figure 1(b) shows

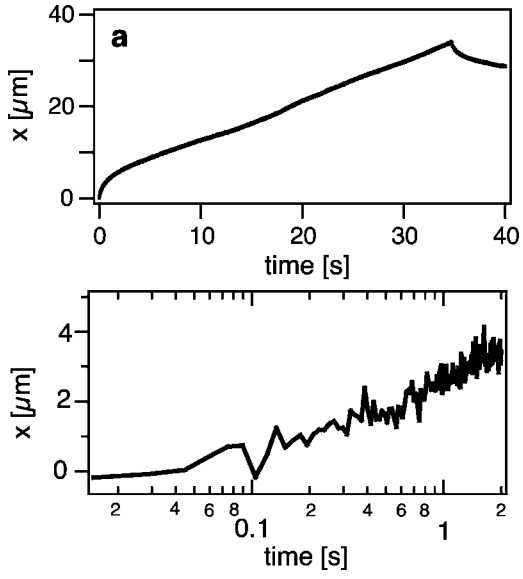

FIG. 1. Displacement of the bead embedded into the actin network under the application of a rectangular force pulse ($c=10$ μM, $f=40$ pN). (b) Initial stages of the enforced bead motion. (Actin concentration $c=11$ μM, force amplitude $f \approx 6.5$ pN).

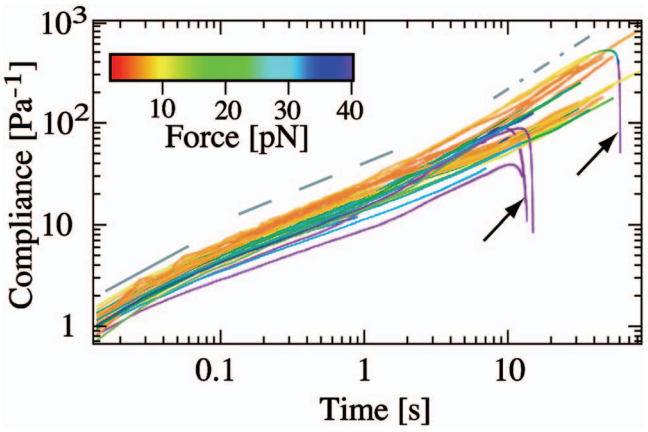

FIG. 2. (Color) Double logarithmic plot of creep compliance *versus* time for various forces superimposed on one graph. The values of the force amplitudes are shown by color running from 3 pN (red) to 40 pN (violet). Three regimes of the bead motion can be distinguished: the short-time regime (a) at $t<\tau_1$ with the slope $\alpha_1 \approx 0.75$ (the solid black line), the intermediate regime (b) with the slope $\alpha_2 \approx 0.5$ taking place at $\tau_1 < t < \tau_2$ (indicated by the dashed black line), and the long-time regime at $t>\tau_2$ characterized by $\alpha_3 \approx 0.9$ (indicated by the dashed-dotted black line). Bending of some curves downward (arrows) takes place, if the bead is close to the core tip of the magnet where the force rapidly increases. Actin concentration is 27 μM.

the initial stage ($0.015 \text{ s} \leqslant t \leqslant 1$ s) of the bead displacement. Figure 2 shows response curves $J=J(t)$ in a double logarithmic scale for different force amplitudes varying from 2 to 40 pN. The force amplitudes are indicated by different colors increasing from red (3 pN) to violet (40 pN). One can distinguish three time regimes of the creep response curves which can be represented by the power law (2). These regimes are separated by two crossover times τ_1 and τ_2, which will be discussed in Sec. III B

B. Crossover times

The crossover times τ_1 and τ_2 mark the transitions between the regimes of the bead motion (Fig. 2). Figure 3 shows the variations of the crossover times with the force applied to the bead. At $f \leqslant 5.5$ pN, the first crossover time τ_1 is independent of the force amplitude [solid line in Fig. 3(a)] and has the value $\tau_1 \approx 0.27 \pm 0.15$ s. At $f > 5.5$ pN, this crossover time decreases with increasing force [dashed line in Fig. 3(a)]. The second crossover time τ_2 decreases with increasing force for all values of the force amplitude [solid line in Fig. 3(b)]. The force dependencies of both crossover times $\tau_1(f)$ (at $f>f_0$) as well as $\tau_2(f)$ (at 2 pN $\leqslant f \leqslant 120$ pN) to a good approximation can be represented by the power laws

$$\tau_{1,2} \sim f^{-\delta_{1,2}}. \tag{3}$$

The exponents for both crossover times are about equal: $\delta_1 \approx \delta_2 \approx 0.5 \pm 0.2$.

The ratio of the crossover times τ_2/τ_1 characterizes the duration of the intermediate regime, while its logarithm, $n=\ln(\tau_2/\tau_1)$, is a measure of the number of time decades

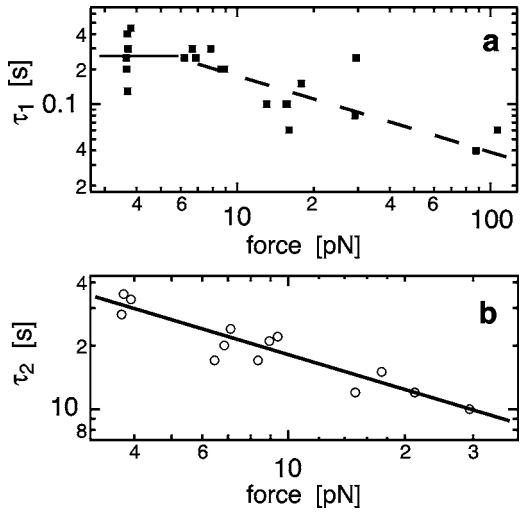

FIG. 3. Crossover times plotted *versus* the force amplitude. (a) The first crossover time τ_1 is force independent at $f \lesssim 9.5$ pN and takes the value $\tau_1 \approx 0.27$ s (solid line). At $f > 9.5$ pN, its dependence on force can be approximated by the power law $\tau_1 \sim f^{-\delta_1}$ (the dashed line). (b) The second crossover time exhibits $\tau_2 \sim f^{-\delta_2}$ dependence on force (solid line) in the whole force interval with $\delta_1 \approx \delta_2 \approx 0.5$.

covered. The data summarized in Fig. 3 yielded $\tau_2/\tau_1 \sim 100$ and $n \approx 2$. Hence, the duration of the intermediate-time regime (the primary interest of the present paper) is two decades.

C. Exponents

If $\ln[J(t)]$ is plotted versus $\ln t$ (Fig. 2), all curves during the short-time ($t < \tau_1$), the intermediate-time ($\tau_1 < t < \tau_2$), and the long-time regimes ($t > \tau_2$) increase nearly linearly. By averaging the slopes in each regime over all curves, we find the exponents

$$\alpha_1 \approx 0.75 \pm 0.05, \quad \alpha_2 \approx 0.5 \pm 0.05, \quad \alpha_2 \approx 0.9 \pm 0.1. \tag{4}$$

The intermediate regime characterized by the exponent α_2 (4) was found in all our measurements, i.e., for all values of the actin concentration and force amplitudes. It was also observed in experiments performed with smaller beads of 2.8 μm diameter (data not shown).

D. Compliance coefficient in the short-time regime

To analyze the creep compliance in the short-time regime, we took into account the uncertainty in the position of the initial data point as described above. Observation of the short-time behavior was possible for forces below 40 pN, since at higher forces the number of data points was too small. All the data obtained in this regime exhibited considerable variations. We averaged the responses obtained from over 20 beads to which 2 to 4 pulses were applied. Figure 4 shows two examples of the averaged short-time response, $x(t)/f$, obtained for networks with actin concentrations of 11 μM (a) and 19 μM (b). The coefficient A_1 of the compliance is independent of the actin concentration and the applied force and takes the value $A_1 \approx (27.2 \pm 6.1)\mathrm{Pa}^{-1}\,\mathrm{s}^{-3/4}$.

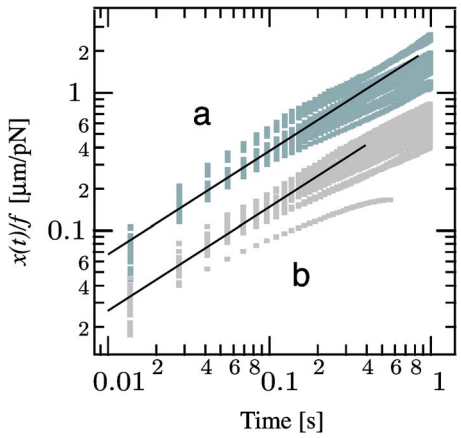

FIG. 4. (Color online) The ratio $x(t)/f$ in the short-time regime for the actin networks with the concentration of 11 μM (a) and 19 μM (b). The marked by grey dots data were obtained by analyzing the responses of 22 (a) and 23 (b) beads. The straight solid lines show the best fit to the power law $x(t)/f \sim t^{\alpha_1}$ for $\alpha_1 = \frac{3}{4}$.

E. Compliance coefficient in the intermediate-time regime

1. Dependence of A_2 on force

Figure 5 shows the compliance coefficient A_2 plotted *versus* the force amplitude for four data sets. The data shown in Figs. 5(a) and 5(c) with concentrations 11 μM (circles), 19 μM (squares), and 27 μM (triangles) correspond to the same day of preparation, while the data shown in Fig. 5(d) ($c = 10$ μM) were obtained from the actin network prepared on a different day. The data shown in Figs. 5(a) and 5(d) are force independent at $f \lesssim 3.1$ pN [Fig. 5(a)] and $f \lesssim 9.5$ pN [Fig. 5(d)] (dashed lines). The data shown in Figs. 5(b) and 5(c) were obtained at higher forces where a force-independent behavior could not be definitely established. The dashed lines in these cases indicate the expected force-independent behavior and yield the following values for A_2: (a) 74 ± 2 $\mathrm{Pa}^{-1}\,\mathrm{s}^{-1/2}$, (b) 28 ± 1 $\mathrm{Pa}^{-1}\,\mathrm{s}^{-1/2}$, (c) 20.1 ± 0.6 $\mathrm{Pa}^{-1}\,\mathrm{s}^{-1/2}$, and (d) 13 ± 1 $\mathrm{Pa}^{-1}\,\mathrm{s}^{-1/2}$. The higher-force dependence of A_2 can be approximated with good accuracy by the power law

$$A_2 \sim f^{-\beta_2}. \tag{5}$$

The exponents β_2 corresponding to the data obtained during the same day of preparation are summarized in Table II. These exponents are averaged using the weighted average method. The resulting value of the exponent is $\beta_2 \approx 0.27 \pm 0.03$.

2. Dependence of A_2 on the actin concentration

Equation (2) predicts that within the intermediate regime, the compliance $J(t)$ depends on the concentration only through the coefficient $A_2 = A_2(c)$. To obtain the highest possible number of data points, one should use data taken simul-

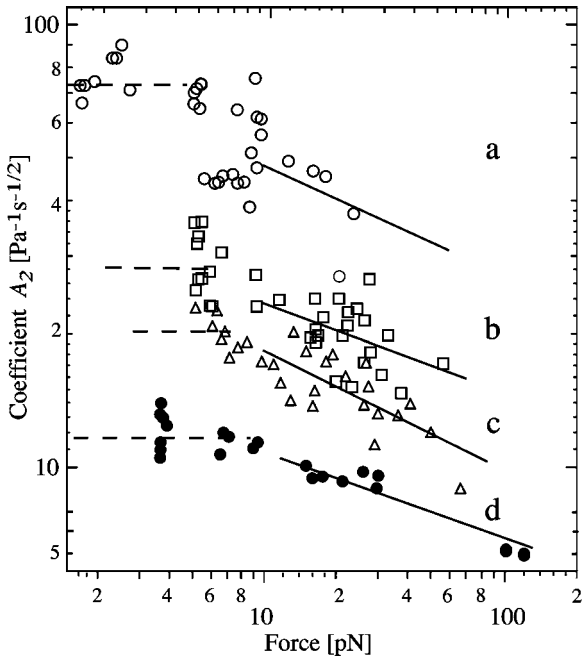

FIG. 5. The compliance coefficient A_2 plotted *versus* force for four concentrations (a) $c=11$ μM (circles), (b) $c=19$ μM (squares), (c) $c=27$ μM (triangles), and (d) $c=10$ μM (filled circles). The first three samples where prepared at the same time and the fourth on another day. A_2 is force independent at small forces [which can be clearly seen in (a) and (d) (dashed lines)], while at higher forces it decreases monotonically with increasing force which can be described by the power law (5). The solid lines show the fits of the corresponding data by the power law (5) yielding the exponents summarized in Table II.

taneously at various values of the force amplitude f. For these purposes, note that one can roughly describe the $A_2=A_2(f)$ dependence using the power law $A_2(f)\sim f^{-0.27}$ over the entire force interval 2 pN$<f<$120 pN. The product $A_2(f)\times f^{0.27}$ is, therefore, approximately force independent and depends only on the actin concentration. This dependence is shown in Fig. 6(a), where each data point represents an average over a series of measurements collected from several tens of pulses and different beads at a given actin concentration. By analyzing the data of Fig. 6(a) in terms of a power law

$$A_2 \sim c^{-\gamma_2}, \tag{6}$$

we find a value of $\gamma_2 \approx 1.1 \pm 0.3$ [the solid line fitting the data in Fig. 6(a)].

TABLE II. Exponents β_2

	Concentration (μM)	Exponent β_2	Error $\delta\beta_2$
	9.5	0.27	0.15
	11	0.35	0.09
	19	0.26	0.04
	27	0.27	0.05
	35	0.31	0.3
Weighted average		0.27	0.03

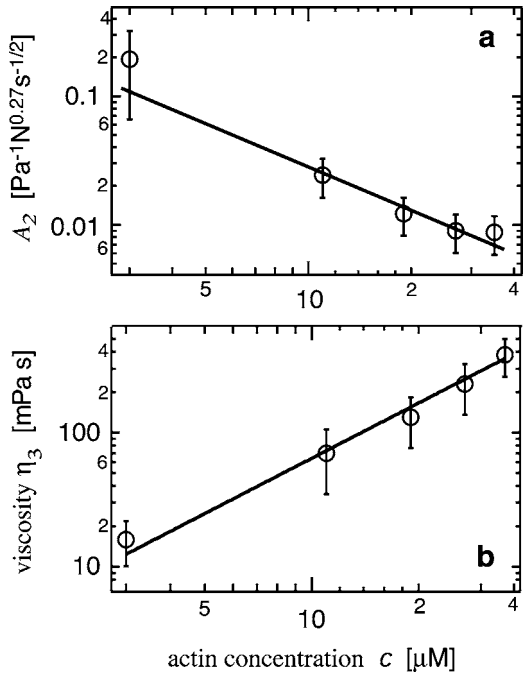

FIG. 6. Variation of the creep compliance of the actin network with the concentration of actin. (a) The force-independent combination $A_2 f^{0.27}$ plotted *versus* concentration in the intermediate regime. Solid line represents the weighted best fit of the data with the power law (6) yielding $\gamma_2 \approx 1.1$. (b) Dependence of the viscosity in the long-time regime η_3 on the actin concentration. Solid line shows the best fit with the power law (8) yielding $\gamma_3 \approx 1.4$.

F. Viscosity in the long-time regime

In the long-time regime ($i=3$), the bead exhibited a steady motion and, therefore, the network could be characterized by the viscosity η_3. Making use of (1) and (2), one finds

$$A_3 \equiv \eta_3^{-1}. \tag{7}$$

In Fig. 6(b), the viscosity η_3 is plotted *versus* the actin concentration. As in the previous case, each data point represents the average over a series of measurements performed with several tens of pulses and different beads for a given network concentration. By analyzing the data in terms of the power law

$$\eta_3 \sim c^{\gamma_3}, \tag{8}$$

we find a value $\gamma_3 \approx 1.4 \pm 0.3$.

G. Viscoelastic modulus of the actin network

Viscoelastic modulus in the time domain $G(t)$ complimentary to the compliance is defined according to the general relation [43] $\int_{-\infty}^{t} G(t-t')J(t')dt' = t$. Taking into account the definition [44] of the viscoelastic modulus in the frequency domain $G(\omega)$, this relation yields

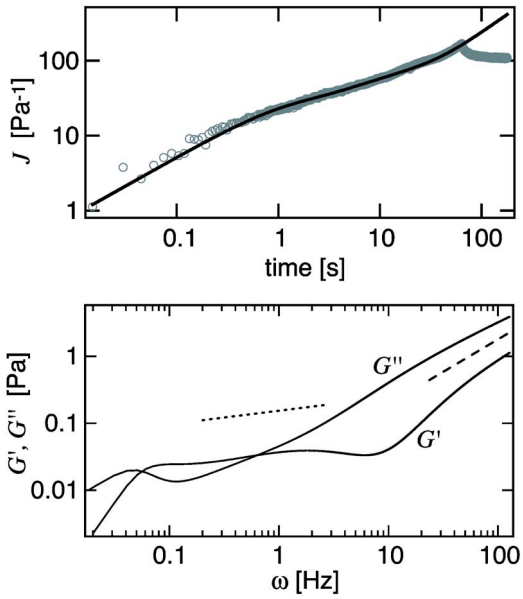

FIG. 7. (Color online) (a) Creep compliance of the network with the concentration $c=10\ \mu$M obtained with the force amplitude $f=17$ pN. The open circles show the experimental data. The solid line shows its fitting by equations (10) and (11). (b) The viscoelastic modulus calculated from the data shown in (a) using representation (15)–(20) and the values of the parameters obtained from the fit. The straight dashed line approximates the behavior of the storage modulus in the plateau regime by the power law $G'(\omega)\sim\omega^{k_2}$ with $k_2\approx 0.1$.

$$G(\omega)=\frac{1}{i\omega\tilde{J}(i\omega)}, \tag{9}$$

where $\tilde{J}(s)=\int_0^\infty J(t)\exp(-ts)dt$ is the Laplace transform of the compliance, s is a complex number, $\tilde{J}(i\omega)\equiv\tilde{J}(s)_{s=i\omega}$ and ω is the frequency. Relation (9) enables one to determine $G(\omega)$, if the Laplace transform of the compliance is calculated. In order to obtain $\tilde{J}(s)$, it is convenient to use a continuous expression approximating the measured compliance instead of the piecewise-continuous function (2). This expression takes the form

$$J(t)=\sum_{i=1}^{3}J_i(t) \tag{10}$$

with

$$J_1(t)=A_1t^{3/4}\exp(-t/\tau_1),\quad J_2(t)=A_2t^{1/2}\exp(-t/\tau_2)\times[1-\exp(-t/\tau_1)],$$

$$J_3(t)=(b_3+A_3t)[1-\exp(-t/\tau_2)]. \tag{11}$$

The three terms (11) of the compliance (10) correspond to the short-time, intermediate-time, and long-time regimes. The exponential factors provide smooth cutoffs of each of these terms outside of the corresponding time interval.

Figure 7(a) shows the compliance data (circles) which were obtained from the network with the actin concentration $c=10\ \mu$M, $f=17$ pN. Fitting of the data by the expressions (10) and (11) yields the solid line. The values of parameters $A_{1,2,3}, b_3$, and $\tau_{1,2}$ found by this fitting are close to those obtained by using of the piecewise-continuous function (2). One can see that (10) and (11) fit the experimental curve with a good accuracy.

Representation of the compliance in the time domain in the form (10) and (11) is favorable, since it enables us to evaluate the Laplace transform of the compliance analytically and, therefore, to calculate the frequency-dependent shear modulus explicitly. The Laplace transform of the sum (10) takes the form $\tilde{J}(s)=\tilde{J}_1(s)+\tilde{J}_2(s)+\tilde{J}_3(s)$, where $\tilde{J}_i(s)$ are the Laplace transforms of the compliance components (11). One finds

$$\tilde{J}_1(s)=\frac{A_1\Gamma(7/4)}{(s+\tau_1^{-1})^{7/4}}, \tag{12}$$

$$\tilde{J}_2(s)=\frac{A_2\pi^{1/2}}{2}\left[\frac{1}{(s+\tau_2^{-1})^{3/2}}-\frac{1}{(s+\tau_3^{-1})^{3/2}}\right], \tag{13}$$

$$\tilde{J}_3(s)=\frac{\tau_2^{-1}}{s^2(s+\tau_2^{-1})^2}[b_3s(s+\tau_2^{-1})+A_3(2s+\tau_2^{-1})], \tag{14}$$

where $\tau_3=\tau_1\tau_2/(\tau_1+\tau_2)$ and the value of the gamma function is $\Gamma(7/4)\approx 0.92$.

Setting $s=i\omega$ in (12)–(14) one can calculate the viscoelastic modulus, $G^*(\omega)=G'(\omega)+iG''(\omega)$. Using (12)–(14), one can express the storage and loss moduli, $G'(\omega)$ and $G''(\omega)$, in terms of auxiliary functions $R(\omega)$ and $I(\omega)$ as

$$G'(\omega)=\frac{R(\omega)}{R^2(\omega)+I^2(\omega)},\quad G''(\omega)=-\frac{I(\omega)}{R^2(\omega)+I^2(\omega)}, \tag{15}$$

where $R(\omega)=R_1(\omega)+R_2(\omega)+R_3(\omega)$, $I(\omega)=I_1(\omega)+I_2(\omega)+I_3(\omega)$, and

$$R_1=\frac{A_1\Gamma(7/4)\omega}{(\omega^2+\tau_1^{-2})^{7/8}}\sin(7\varphi_1/4),\quad I_1=\frac{A_1\Gamma(7/4)\omega}{(\omega^2+\tau_1^{-2})^{7/8}}\cos(7\varphi_1/4), \tag{16}$$

$$R_2=\frac{A_2\pi^{1/2}\omega}{2}\left[\frac{\sin(3\varphi_2/2)}{(\omega^2+\tau_2^{-2})^{3/4}}-\frac{\sin(3\varphi_3/2)}{(\omega^2+\tau_3^{-2})^{3/4}}\right], \tag{17}$$

$$I_2=\frac{A_2\pi^{1/2}\omega}{2}\left[\frac{\cos(3\varphi_2/2)}{(\omega^2+\tau_2^{-2})^{3/4}}-\frac{\cos(3\varphi_3/2)}{(\omega^2+\tau_3^{-2})^{3/4}}\right], \tag{18}$$

$$R_3=\frac{b_3\tau_2^{-2}(\omega^2+\tau_2^{-2})-2A_3\tau_2^{-1}\omega^2}{(\omega^2+\tau_2^{-2})^2}, \tag{19}$$

$$I_3=-\frac{b_3\omega}{\tau_2(\omega^2+\tau_2^{-2})}-\frac{A_3(3\omega^2+\tau_2^{-2})}{\omega\tau_2^2(\omega^2+\tau_2^{-2})^2}. \tag{20}$$

Here, $\varphi_i=\arctan(\omega\tau_i)$, $i=1, 2, 3$. Though these are rather complex, equations (15)–(20) yield the storage and loss

moduli in an explicit form. Since the parameters $A_1, A_2, A_3, b_3, \tau_1$, and τ_2 are obtained by fitting the compliance curve defined by Eqs. (10) and (11), the expressions (15)–(20) contain no undefined parameters. Using a double logarithmic scale, Fig. 7(b) shows the storage and loss moduli, $G'(\omega)$ and $G''(\omega)$, obtained using (15)–(20).

It is clearly seen that the three regimes of $J(t)$ in the time domain (presented in Fig. 2) map onto three frequency regimes of $G'(\omega)$ [Fig. 7(b)]: the high-frequency, the low-frequency and the intermediate-frequency (usually referred to as the plateau) regimes. On the double-logarithmic plot [Fig. 7(b)], the dependence of the storage modulus on frequency in the plateau regime is close to a straight line and can be approximately characterized by its slope k_2. By fitting, we find $k_2 \approx 0.1 \pm 0.15$.

IV. DISCUSSION

A. Compliance of actin networks in the time domain

We studied the viscoelastic properties of entangled actin networks of various concentrations by magnetic bead microrheometry. Using rectangular force pulses of up to 60-s duration enabled us to observe three distinct types of the bead motion, referred to as the short-time, the intermediate-time, and the long-time regimes separated by crossover times τ_1 and τ_2. Each regime can be described by the expression (2).

During the short-time regime ($t \leqslant \tau_1 \sim 0.1$ s), we observed the bead motion described by the well-known exponent $\alpha_1 = 0.75$ [14,28,36,37,45–47]. The bead displacement during the short-time regime is smaller than the mesh size [cf. Fig. 1(b) and Table I] and, from this, we deduce that the bead encounters only few actin filaments. Due to the structural inhomogeneity of the network, the number of filaments encountered varies from bead to bead. This explains the observed variations in the compliance coefficient A_1. The model proposed in the paper [28] accounting for the dynamic bending of filaments by the bead, describes the bead motion in this regime. Estimates made in Ref. [48] show that this model exhibits a good agreement with our measurements.

The short-time regime is followed by the intermediate-time regime at $\tau_1 < t < \tau_2$ which covers two decades. This regime is characterized by the power law $J(t) \sim t^{\alpha_2}$ with $\alpha_2 \approx 0.5$ for all actin concentrations and all force amplitudes. This is the first observation of the regime characterized by the square-root time dependence $\alpha_2 \approx 0.5$ during forced bead motion, and therefore, this regime is in the main focus of our interest in this paper. For $f \leqslant f_0 \approx 9.5$ pN, where we found that the compliance does not depend on the force, we determined a power law $J(t) \sim t^{\alpha_2} c^{-\gamma_2}$ with $\gamma_2 \approx 1.1$. Thus at $f \leqslant f_0$, the bead displacement depends linearly on the force amplitude $x(t) \sim t^{\alpha_2} c^{-\gamma_2} f$. In contrast, at higher forces ($f > f_0$), the compliance decreases with increasing force, such as $J(t) \sim t^{\alpha_2} c^{-\gamma_2} f^{-\beta_2}$, and the displacement exhibits a sublinear force dependence $x(t) \sim t^{\alpha_2} c^{-\gamma_2} f^{1-\beta_2}$ with $\beta_2 \approx 0.27$. The origin of such a nonlinearity may be related to an orientational ordering of filaments in the vicinity of the moving bead as well as to a weak cross-linking of the filaments (for example, by divalent ions always present in the solution). Identifying its origin is, however, outside the scope of this work.

The intermediate regime can only be observed provided $\tau_{\max}/\tau_1 \gg 1$. In previous works [7,8,13,26,29,32,38,49,50], pulses with shorter duration (typically $\tau_{\max} \sim 1$ s) were used. In that case, $\tau_{\max}/\tau_1 \approx 3$–$10$, a ratio insufficiently large to clearly detect the intermediate regime. In the present work, we used pulses with much longer duration ($\tau_{\max}$ up to 60 s which yields $\tau_{\max}/\tau_1 \sim 10^2$–$10^3$). This enabled us to reliably observe the intermediate regime.

At $t > \tau_2$, we observed a crossover to the behavior $J(t) \sim c^{-\gamma_3} t^{\alpha_3}$ with $\alpha_3 \approx 0.9$ indicating a viscouslike motion and $\gamma_3 \approx 1.4$. A simple calculation $\ln(\tau_{\max}/\tau_2) \approx 0.78$ shows that we observed the long-time behavior over less than a decade. In principle, this is not long enough to reliably establish the value of the exponent α_3, if it were unknown. It is generally expected that on a long-time scale, entangled actin networks must exhibit viscouslike behavior described by $J(t) \sim t$ yielding $\alpha_3 = 1$. We believe, however, that at $t > \tau_2$, we are observing the transition to a viscouslike behavior of the network. Two considerations support the conclusion that there are no other regimes between the intermediate-time and the viscouslike long-time one. First, the overall bead displacement [i.e., $x_{\max} = x(\tau_{\max})$] is much larger than the mesh size, and the network properties are effectively averaged over such a distance. Thus, a further increase of $\tau_{\max}$ (accompanied by the increase of the $x_{\max}$) cannot yield new information about the network. Second, macrorheometric and microrheometric measurements in the frequency domain at small frequency values did not indicate any other regimes or peculiarities of the viscoelastic moduli at $\omega \lesssim \tau_2^{-1}$ (see, for example, [11,51]). For these reasons, the fact that the exponent α_3 extracted from the compliance curve is close to the expected value $\alpha_3 = 1$ as well as the correspondence of the time interval $t > \tau_2$ to those observed elsewhere [11,51] enables us to state that at $t > \tau_2$, we have observed the transition to the long-time regime in which the compliance is linear in time.

Fluid behavior exhibiting a linear dependence of compliance on time $J(t) \sim t$ is usually referred to as viscous. The term "viscous" assumes, however, a shear-friction mechanism of dissipation [52] and the corresponding shear-induced mechanism of the resistance of the fluid to the bead motion. The network resistance to the bead motion is, however, determined by the piling up actin filaments in front of the bead [35,48] (see Sec. IV B), rather than by a shear friction. For this reason, we refer to the long-time regime as being quasiviscous.

B. Comparison with previous results

A behavior related to the intermediate regime has been recently observed by the two-bead microrheology [45]. To discuss this relation, first note that the Laplace transform of the binary correlation function of a freely fluctuating bead (as well as that of its mean square displacement) has the form [21] $\langle x_\omega x_{-\omega} \rangle \sim [\omega G(\omega)]^{-1}$. Comparing this with (9) and making the inverse Laplace transform, one finds

$\langle x^2(t)\rangle \sim J(t)$. Our data lead to the conclusion that in the intermediate-time regime, the mean square displacement of the freely fluctuating bead depended on time as $\langle x^2(t)\rangle \sim t^{1/2}$ in agreement with the observation by means of two-bead microrheometry [45].

At $\tau_1/\tau_2 \ll 0.1$, the second term in (23) is much smaller than the first one, and thus, the slope of the plateau will be close to the value $k_2=0.5$. For this reason, the impedance spectra with $G'(\omega)\sim\omega^{1/2}$ may be an indication of the intermediate regime. Such a dependence has been predicted in the paper [53] for flexible polymers (i.e., with $L/L_p \gg 1$, where L and L_p are the contour and persistent lengths of the filaments). The actin filaments used in our work possess contour length $L\approx 20\ \mu$m and persistent length $L_p \approx 17\ \mu$m [54]. They are thus, semiflexible with $L/L_p \approx 1.2$. For this reason, the mechanism discussed in Ref. [53] is not responsible for the intermediate-time behavior of the network reported in the present work.

Simulation of the forced motion of a bead through a network of semiflexible filaments was reported recently [55]. These simulations exhibited the short-time and intermediate-time regimes characterized by the exponents $\alpha_1 \approx 0.75$ and $\alpha_2 \approx 0.5$. They predicted that in the intermediate regime, the bead displacement obeys the power law $x(t)\sim t^{0.5}c^{-1.4}f$. The simulation revealed also the following mechanism responsible for the resistance of the network to the bead motion during the intermediate regime. The filaments are piled up in front of the moving bead, and steric repulsion between the bead and the filaments makes the main contribution to the resisting force. Because of limitations of the simulation time, the long-time regime was not observed in Ref. [55].

The intermediate-time and long-time regimes with $\alpha_2=\frac{1}{2}$ and $\alpha_3=1$ have been predicted by an analytical theory [35,48]. This approach [35,48] yields estimates for the compliance coefficients A_2 and A_3

$$A_2 \approx 6\pi\chi_2 \frac{L_p^{1/3}\xi^{8/3}D^{1/2}}{Rk_BT}, \quad A_3 \approx 6\pi\chi_3 \frac{4L_p^{1/3}\xi^{8/3}D}{R^2k_BT}, \quad (21)$$

where D is the longitudinal diffusion coefficient of the filaments, T is the temperature, and $\chi_{2,3}$ are dimensionless geometrical factors taking on the values $\chi_2 \approx 0.055$ [55] and $\chi_3 \approx 0.04$ [48]. In Refs. [35,48], both A_2 and A_3 are independent of the force amplitude (i.e., $\beta_2=\beta_3=0$), which agrees with the behavior of A_2 at $f \leqslant f_0$ as well as of A_3 observed in the present work. Since $\xi\sim c^{-1/2}$, Eq. (21) predicts $\gamma_2=\gamma_3=\frac{4}{3}$ close to the values $\gamma_2\approx 1.1$ and $\gamma_3\approx 1.4$ reported here. Taking the parameters $\xi\approx 0.5\ \mu$m (corresponding to the actin concentration $c=11\ \mu$M), $R=2.25\ \mu$m of our system, the diffusion coefficient [56] $D\sim 10^{-13}$ m^2/s and $L_p\approx 17\ \mu$m [54], one finds $A_2\sim 10$ Pa^{-1} s$^{-1/2}$. This estimate agrees well with one of the values of $A_2\approx 13\pm 1$ Pa^{-1} s$^{-1/2}$ reported here [Fig. 5(d)]. It is, however, smaller by an order of magnitude than the other values of A_2 reported in this work [Figs. 5(a)–5(c)]. These three values, however, derive from measurements carried out on preparations made on a day different from that on which the fourth measurement was made. Finally, one finds the estimate for the coefficient of the long-time regime $A_3\sim 1$ Pa^{-1} s^{-1}, which is smaller than the coefficient $A_3=\eta_3^{-1}\approx 10$ Pa^{-1} s^{-1} reported in this work [cf. Fig. 6(b) at $c=11\ \mu$M].

The discrepancy between the observations corresponding to different days of preparation of the network (and the corresponding discrepancy between the experimental results and the theoretical predictions) are related to the highly inhomogeneous structure of the actin gel, which cannot be controlled simultaneously with the micromechanical measurements. During the network preparation, the probe beads are more easily embedded into less dense regions of the network and, therefore, exhibit higher displacement (yielding higher A_2 values) than would be obtained for a homogeneous gel.

C. Viscoelasticity of actin networks in the ω domain

The frequency-dependent viscoelastic modulus obtained from our compliance data also exhibited three regimes which could be related to the three types of behavior observed in the time domain.

To approximate the cumbersome formulas (15)–(20) by a simple analytical expression for the plateau modulus, we introduced a frequency $\omega_0=(\tau_1\tau_2)^{1/2}$ lying in the middle of the logarithmic frequency interval $[\ln(\tau_2^{-1}),\ln(\tau_1^{-1})]$. Since in our measurements, the inequality $\tau_2^{-1} \ll \omega_0 \ll \tau_1^{-1}$ holds in the vicinity of ω_0, one can neglect $R_1(\omega), R_3(\omega), I_1(\omega)$, and $I_3(\omega)$ with respect to $R_2(\omega)$ and $I_2(\omega)$ in (15). Neglecting, in addition, small terms $\sim\omega_0\tau_1$ and $(\omega_0\tau_2)^{-1}$, one finds the approximate values of the moduli in the middle of the plateau

$$G'(\omega_0)\approx G''(\omega_0)\approx \frac{1}{A_2(\tau_1\tau_2)^{1/4}}\left(\frac{2}{\pi}\right)^{1/2}. \quad (22)$$

From (6) and (22), it follows that the plateau modulus depends on the actin concentration as $G'(\omega_0)\sim G''(\omega_0)\sim c^{\gamma_2}$. Our results yield $\gamma_2\approx 1.1$, while the theoretical approach [35,55] predicts $\gamma_2\approx\frac{4}{3}$.

The exponent k_2 describing the plateau slope can also be calculated within the approximation $R(\omega)\approx R_2(\omega)$, $I(\omega)\approx I_2(\omega)$. However, in this case, as we will see, the exponent k_2 is small and the terms $\sim\omega_0\tau_1$ and $(\omega_0\tau_2)^{-1}$ appear to be comparable with its magnitude so that the previous approximation cannot be applied. Accordingly, we calculated k_2 numerically as $k_2=\langle d\ln G'(\omega)/d\ln\omega\rangle$, where the derivative is averaged over the interval of the monotonicity of $G'(\omega)$. The exponent k_2 can be approximated by the expression

$$k_2 \approx 0.5 - 0.8(\tau_1/\tau_2)^{1/4}. \quad (23)$$

The high-frequency end of the plateau ω_h is determined by the condition [11]

$$G'(\omega_h)=G''(\omega_h). \quad (24)$$

Evidently, the value ω_h is of the order of τ_1^{-1}. In this case, one can neglect $R_3(\omega)$ and $I_3(\omega)$ with respect to $R_1(\omega), R_2(\omega), I_1(\omega)$, and $I_2(\omega)$ in (15). In this approximation, Eq. (24) takes the form

$$\frac{1}{[(\omega_h\tau_1)^2+1]^{1/8}}\frac{\sin(7\varphi_h/4+\pi/4)}{\sin(3\varphi_h/2+\pi/4)}\approx\frac{\pi^{1/2}}{2\Gamma(7/4)}\frac{A_2}{A_1\tau_1^{1/4}}, \tag{25}$$

where $\varphi_h=\arctan(\omega_h\tau_1)$. In Ref. [48], the first crossover time τ_1 has been defined from the condition that the compliance curve (2) of the short-time regime ($i=1$) intersects with that corresponding to the intermediate regime ($i=2$) yielding $A_1\tau_1^{3/4}=A_2\tau_1^{1/2}$. This condition reduces the right-hand side of Eq. (25) to $\pi^{1/2}/2\Gamma(7/4)\approx 0.964$. Equation (25) can be then solved numerically yielding the high-frequency end of the plateau $\omega_h\approx 0.549\tau_1^{-1}$.

Substituting $A_2\sim 10\ \mathrm{Pa}^{-1}\ \mathrm{s}^{-1/2}$, $\tau_1\sim 0.1$ s, and $\tau_2\sim 10$ s from our measurements in (22) and (23), one finds $\omega_0\sim 1$ Hz, $k_2\approx 0.25$, $G'(\omega_0)\sim G''(\omega_0)\sim 0.1$ Pa, and $\omega_h\sim 5$ Hz.

Viscoelastic impedance spectra of actin networks obtained by oscillating magnetic bead microrheometry was reported in Ref. [11]. In this paper, networks with actin concentrations $c=12$, 24, and 48 μM, which cover the same range as the concentrations used in our work, were studied. The values of the moduli $G'(\omega_0)$ and $G''(\omega_0)$ in the middle of the plateau interval reported in Ref. [11] are close to our estimates. In Ref. [11], viscoelastic moduli are plotted as a function of frequency $\nu=\omega/2\pi$. Our calculation yields the high-frequency end of the plateau $\nu_h\approx 0.087\tau_1^{-1}\approx 1$ Hz in excellent agreement with the results reported in the paper [11].

Note that in order to characterize the plateau regime, we calculated $G'(\omega_0)\sim G''(\omega_0)$ and k_2 within the approximation in which we neglected $R_1(\omega), R_3(\omega), I_1(\omega)$, and $I_3(\omega)$ with respect to $R_2(\omega)$ and $I_2(\omega)$. In other words, we accounted only for the contribution of the intermediate regime. The good agreement of our calculations with the data shown in Fig. 6(b) ensures that in forced bead microrheology, the intermediate-time regime in the t domain is directly related to the plateau regime of $G'(\omega)$ in the ω domain.

Comparison with the mechanism responsible for the intermediate-time regime [35,55,48] leads to the conclusion that formation of the plateau in microrheological measurements is determined by piling up the filaments by the moving bead and their redistribution by diffusion.

ACKNOWLEDGMENTS

We thank M. Rusp for actin preparations and J. Schilling for providing the image processing software OPENBOX J. U. was supported by the Deutsche Forschungsgemeinschaft, Grant No. SFB 563, and the Fonds der Chemischen Industrie, and A. B. by the Deutsche Forschungsgemeinschaft, Grant No. SA246/28-4. This work was supported in part (D. A. P.) by National Science and Engineering Research Consul of Canada.

[1] B. Alberts *et al.*, *Molecular Biology of the Cell* (Garland Publishing Inc., New York, 1994).
[2] E. A. Evans and R. Skalak, *Mechanics and Thermodynamics of Biomembranes* (CRC Press, Boca Raton, FL, 1980).
[3] M. Radmacher, M. Fritz, and P. K. Hansma, Biophys. J. **69**, 264 (1995).
[4] M. Radmacher, IEEE Eng. Med. Biol. Mag. **16**, 47 (1997).
[5] M. Radmacher *et al.*, Eur. J. Cell Biol. **74**, 38 (1997).
[6] S. C. Kuo, Traffic Eng. **2**, 757 (2001).
[7] F. Ziemann, J. Rädler, and E. Sackmann, Biophys. J. **66**, 2210 (1994).
[8] A. R. Bausch *et al.*, Biophys. J. **75**, 2038 (1998).
[9] F. G. Schmidt, B. Hinner, E. Sackmann, and J. X. Tang, Phys. Rev. E **62**, 5509 (2000).
[10] G. Forgacs, S. A. Newman, B. Hinner, Ch. Maier, and E. Sackmann, Biophys. J. **84**, 1272 (2003).
[11] F. G. Schmidt, B. Hinner, and E. Sackmann, Phys. Rev. E **61**, 5646 (2000).
[12] R. Merkel *et al.*, Biophys. J. **79**, 707 (2000).
[13] L. Vonna *et al.*, J. Cell. Sci. **116**, 785 (2003).
[14] F. C. MacKintosh and C. F. Schmidt, Curr. Opin. Colloid Interface Sci. **4**, 300 (1999).
[15] A. Mukhopadhyay and S. Granick, Curr. Opin. Colloid Interface Sci. **6**, 423 (2001).
[16] T. G. Mason *et al.*, J. Rheol. **44**, 917 (2000).
[17] M. L. Gardel, M. T. Valentine, J. C. Crocker, A. R. Bausch, and D. A. Weitz, Phys. Rev. Lett. **91**, 158302 (2003).
[18] I. Y. Wong, M. L. Gardel, D. R. Reichman, E. R. Weeks, M. T. Valentine, A. R. Bausch, and D. A. Weitz, Phys. Rev. Lett. **92**, 178101 (2004).
[19] G. H. Koenderink *et al.*, Biophys. J. **86**, 360a (2004).
[20] B. Schnurr *et al.*, Biophys. J. **72**, Tu285 (1997).
[21] M. J. Solomon and Q. Lu, Curr. Opin. Colloid Interface Sci. **6**, 430 (2001).
[22] A. Ashkin, ASGSB Bull **4**, 133 (1991).
[23] H. Freundlich and W. Seifriz, Z. Phys. Chem., Stoechiom. Verwandtschaftsl. **104**, 233 (1922).
[24] A. Heilbronn, Jahrb. Radioakt. Elektron. **61**, 284 (1922).
[25] K. S. Zaner and P. A. Valberg, J. Cell Biol. **109**, 2233 (1989).
[26] A. R. Bausch, W. Möller, and E. Sackmann, Biophys. J. **76**, 573 (1999).
[27] F. Amblard *et al.*, Rev. Sci. Instrum. **67**, 818 (1996).
[28] F. Amblard, A. C. Maggs, B. Yurke, A. N. Pargellis, and S. Leibler, Phys. Rev. Lett. **77**, 4470 (1996).
[29] M. A. Dichtl and E. Sackmann, PNAS **99**, 6533 (2002).
[30] M. Keller *et al.*, Philos. Trans. R. Soc. London, Ser. A **361**, 699 (2003).
[31] B. Hinner, M. Tempel, E. Sackmann, K. Kroy, and E. Frey, Phys. Rev. Lett. **81**, 2614 (1998).
[32] F. G. Schmidt, F. Ziemann, and E. Sackmann, Eur. Biophys. J. **24**, 348 (1996).
[33] M. A. Dichtl and E. Sackmann, New J. Phys. **1**, 18.1/18.11 (1999).
[34] M. Keller, J. Schilling, and E. Sackmann, Rev. Sci. Instrum. **72**, 3626 (2001).
[35] J. Uhde, W. Feneberg, N. Ter-Oganessian, E. Sackmann, and

A. Boulbitch, Phys. Rev. Lett. **94**, 198102 (2005).
[36] F. Gittes and F. C. MacKintosh, Phys. Rev. E **58**, R1241 (1998).
[37] F. Gittes, B. Schnurr, P. D. Olmsted, F. C. MacKintosh, and C. F. Schmidt, Phys. Rev. Lett. **79**, 3286 (1997).
[38] W. Feneberg, M. Westphal, and E. Sackmann, Eur. Biophys. J. **30**, 284 (2001).
[39] J. Uhde, PhD Thesis, Technical University of Munich, 2004 (unpublished);http:/tumb1.biblio.tu-muenchen.de/publ/diss/ph/2004/uhde.html
[40] J. A. Spudich and S. Watt, J. Biol. Chem. **246**, 4866 (1971).
[41] S. MacLean-Fletcher and T. D. Pollard, Biochem. Biophys. Res. Commun. **96**, 18 (1980).
[42] T. W. Houk and K. Ue, Anal. Biochem. **62**, 66 (1974).
[43] N. W. Tschoegl, *The Phenomenological Theory of Linear Viscoelastic Behavior* (Springer-Verlag, Berlin, 1989).
[44] M. Doi and S. F. Edwards, *The Theory of Polymer Dynamics* (Oxford University Press, Oxford, 1986).
[45] J. C. Crocker, M. T. Valentine, E. R. Weeks, T. Gisler, P. D. Kaplan, A. G. Yodh, and D. A. Weitz, Phys. Rev. Lett. **85**, 888 (2000).
[46] D. C. Morse, Macromolecules **31**, 7030 (1998).
[47] R. Granek, J. Phys. II **7**, 1761 (1997).
[48] N. Ter-Oganessian, D. A. Pink, and A. Boulbitch, Phys. Rev. E **72**, 041511 (2005).
[49] W. Feneberg and E. Sackmann, Cell. Mol. Biol. Lett. **6**, 201 (2001).
[50] F. Schmidt, PhD Thesis, Technical University of Munich, 1999 (unpublished).
[51] R. Ruddies *et al.*, Eur. Biophys. J. **22**, 309 (1993).
[52] L. D. Landau and E. M. Lifshitz, *Fluid Mechanics* (Pergamon Press, Oxford, 1987).
[53] D. C. Morse, Macromolecules **31**, 7044 (1998).
[54] F. Gittes *et al.*, J. Cell Biol. **120**, 923 (1993);A. Ott, M. Magnasco, A. Simon, and A. Libchaber, Phys. Rev. E **48**, R1642 (1993).
[55] N. Ter-Oganessian, D. A. Pink, B. Quinn, and A. Boulbitch, Phys. Rev. E **72**, 041510 (2005).
[56] M. Dichtl and E. Sackmann (unpublished).